Bulletin of the Seismological Society of America, Vol. 94, No. 6, pp. 2028–2036, December 2004

The Effect of Bandwidth Limitations on the Inference of Earthquake Slip-Weakening Distance from Seismograms

by Paul Spudich and Mariagiovanna Guatteri

Abstract Numerous researchers have obtained estimates of slip-weakening distance, D_c, and fracture energy for recent earthquakes. D_c is often observed to be a significant fraction of the total slip and tends to correlate with total slip. Although these observations may well be true of real earthquakes, we show that low-pass filtering of strong-motion seismograms can also produce some of these effects in inverted rupture models. We test the accuracy of D_c estimates by calculating them in low-pass-filtered versions of models A and B of Guatteri and Spudich (2000). Models A and B are two different rupture models for a hypothetical M 6.5 earthquake, and they have nearly identical rupture time, slip, and stress-drop distributions, and nearly identical predicted seismograms, but D_c for model B is about twice that for model A. By low-pass filtering slip models A and B at 1.0 Hz, we simulate the blurring effects of band-limited waveform inversions on these slip models. At each point on a fault, D_c' is defined to be the slip at the time of the peak slip speed at that point. Low-pass filtering the slip models causes an upward bias in D_c inferred from stress-slip curves, and it causes an artificial correlation between D_c' and the total slip. Low-pass filtering might also bias fracture energy high and radiated energy low. These biases should be considered when interpreting D_c derived from band-limited slip models of real earthquakes.

Introduction

A major research goal of strong-motion seismology is the inference of the frictional properties of faults during dynamic rupture, where by "frictional properties" we mean the dependence of frictional traction on slip, slip speed, temperature, pressure, permeability, past history, and any other related variables. Seismologists have attempted to learn about fault friction during earthquake dynamic slip by applying various inversion techniques to observed earthquake seismograms (e.g., Fukuyama and Mikumo, 1993; Ide and Takeo, 1997), but the inference of frictional properties is impeded by poor spatial and temporal resolution in the ground-motion inversions (Ide and Takeo, 1997).

Guatteri and Spudich (2000) proposed that fracture energy G_c might be reliably inferred from ground-motion inversions, despite the frequency band limitations. They presented two rupture models, models A and B, having very similar ground motions and spatial distributions of slip, static stress drop, rupture time, and G_c, but different distributions of slip-weakening distance D_c and yield stress. From this they inferred that D_c could not be reliably estimated from inversion of band-limited strong ground-motion data typical of most earthquake ground-motion data sets.

Mikumo *et al.* (2003) and Fukuyama *et al.* (2003) have proposed a parameter they call D_c', which can be easily calculated from a kinematic slip model without requiring calculation of the associated stress changes and which might be a useful estimate of D_c, although they note that in some cases it must be corrected. At each point on a fault, D_c' is defined to be the total slip at the time of the peak slip speed at that point. In other words, if $D(x,t)$ is the slip at point x and time t, and if $v(x,t)$ is the slip speed at x and t, and $T(x)$ is the time at which $v(x,t)$ reaches its maximum value at point x, then $D_c'(x) = D(x,T(x))$. An example is given in Figure 1. Note that the resolution of D_c' is limited by the granularity of the time sampling.

Mikumo *et al.* (2003) have calculated D_c' values for two types of slip models, those obtained from numerical simulations of spontaneous rupture and those obtained from inversions of ground-motion data. The different time resolution of the two types of slip models is a critical distinction. The first type of slip model, if derived from a sufficiently densely time-sampled calculation, successfully resolves the weakening process in time. For brevity we will call this type of model "temporally resolved." However, a slip model derived from band-limited ground-motion data might not contain modeled periods shorter than the breakdown time (the duration of weakening at a point on the fault). We will use the term "temporally unresolved" to describe a slip model

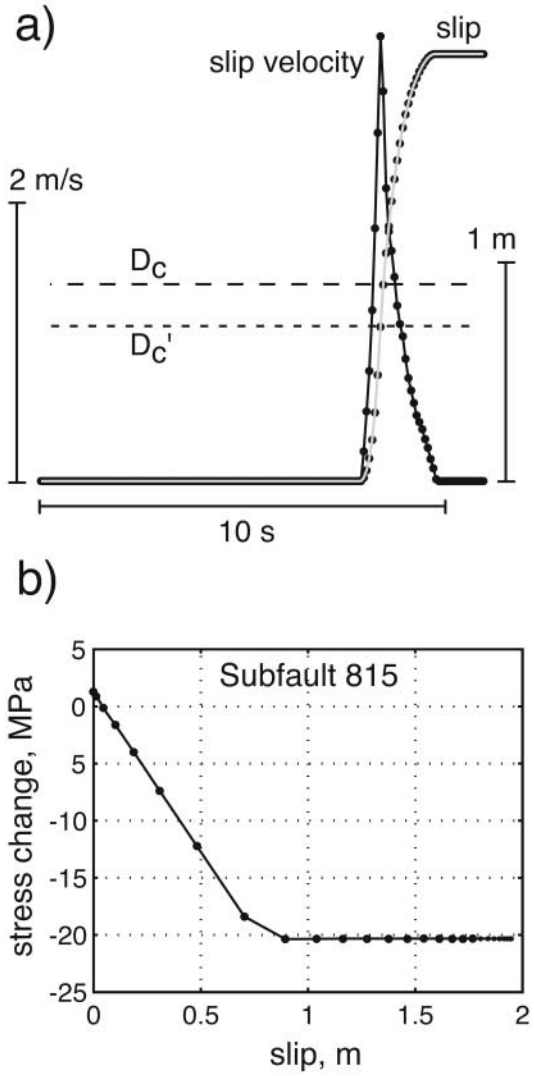

Figure 1. Various quantities at subfault 815, located 20 km along strike, 10.4 km downdip, in model B of Guatteri and Spudich (2000). (a) Dislocation and slip speed as a function of time. Long dashed line shows D_c and short dashed line shows D_c'. (b) Stress change versus slip. Dots are points calculated at each time step in the numerical simulation; lines are a linear interpolant.

that lacks modeled periods shorter than the breakdown time. Typically, when performing a ground-motion inversion, the investigator does not know whether the obtained slip model is temporally resolved.

The concept of "modeled periods" is crucial to determining whether an inverted slip model is temporally resolved or unresolved. Cotton and Campillo's (1995) inverted slip model of the 1992 Landers earthquake illustrates the concept of modeled periods well. Although Cotton and Campillo bandpass filtered their ground-motion data between 0.05 and 0.5 Hz, their figure 5 shows that their model fit the data well (variance reduction more than 30%, an arbitrarily chosen threshold) only between the frequencies of 0.065 and 0.2 Hz. Thus, the shortest modeled period in their data is 5 sec. Consequently, if the true Landers breakdown time is greater than 5 sec, then Cotton and Campillo's slip model is temporally resolved. Cotton and Campillo explicitly applied a bandpass filter with corners at 0.05 and 0.5 Hz, and all the other blurring factors in the inversion implicitly filtered the slip model with a bandpass filter having corners 0.065 and 0.2 Hz.

Using results and procedures developed by Ide and Takeo (1997), Guatteri and Spudich (2000), Mikumo *et al.* (2003), and Fukuyama *et al.* (2003), numerous researchers have obtained estimates of D_c and fracture energy for recent earthquakes. Certain common features have been observed. D_c is often observed to be a significant fraction of the total slip (e.g., Ide and Takeo, 1997; Day *et al.*, 1998), although these investigators acknowledge that resolution limits might affect their results. Mikumo *et al.* (2003) and Zhang *et al.* (2003) have found that D_c, derived from D_c', tends to correlate with total slip in the 2000 Tottori, Japan, and the 1999 Chi-Chi, Taiwan, earthquakes. Although these observations may well be true of real earthquakes, in this article we will show that low-pass filtering of strong-motion seismograms can also produce some of these effects.

The objective of our article is to investigate the effects of limited bandwidth on the inference of slip-weakening distance and fracture energy from kinematic rupture models derived from observed ground-motion data. Such kinematic rupture models have reduced resolution because of anelastic attenuation in the Earth, inaccurate Green's functions, low-pass filters typically applied by the investigators, poor spatial resolution caused by a limited number of observation locations, coarse discretization required by computational limitations, and other factors. Rather than trying to simulate all these blurring factors, we will choose two numerical dynamic-rupture models and investigate just the effect of one of the factors, low-pass filtering the associated slip-velocity and stress time series. In essence, our filtered dynamic-rupture models are equivalent to kinematic ground-motion inversions having perfect spatial resolution and perfect Green's functions but limited time resolution. More specifically, if slip-velocity model $v(x,t)$ and associated stress change $\tau(x,t)$, both defined over the whole fault, cause ground motions $u(y,t)$, and if $f(t)$ is a time-domain convolution filter, then $f(t)*v(x,t)$ and $f(t)*\tau(x,t)$ are the slip-velocity and stress-change models that cause ground motions $f(t)*u(y,t)$, owing to the linearity of the relation between slip velocity, stress change, and ground motion. If $f(t)$ is chosen so that $f(t)*v(x,t)$ is nonnegative, then $f(t)*v(x,t)$ satisfies all the criteria for a valid rupture model for data $f(t)*u(y,t)$. If the inferred slip-weakening distance is poorly resolved in our filtered dynamic models $f(t)*v(x,t)$ and $f(t)*\tau(x,t)$, it will necessarily be even worse in kinematic slip models derived from real data. We will show that low-pass filtering a slip model tends to bias stress-slip curves to larger values of D_c, it introduces an artificial correlation of D_c' with

maximum slip, and it might bias fracture energy high and radiated energy low.

Application to Models A and B

We will answer these questions by calculating D_c and D_c' in unfiltered and low-pass-filtered versions of models A and B of Guatteri and Spudich (2000). Models A and B are two different rupture models [by which we mean $D(x,t)$] of a hypothetical M 6.5 earthquake source. These rupture models were derived from a constrained optimization technique in which they were constrained by a mixture of required conditions on slip and stress. They were required to have similar spatial rupture time distributions, moment rate functions, and upper bounds on stress drop over a given rupture area. Their slip $D(x,t)$ was related to stress change $\tau(x,t)$ through the integral relations (15) to (16) in Das and Kostrov (1987) and the unloading relation (18) of Andrews (1985). Model A was required to weaken more rapidly than model B. The results of these constraints were two rupture models having spatially variable D_c and having slip-weakening curves that were usually, but not always, linear. In other words, models A and B are proper dynamic rupture models, but with derived, rather than imposed, slip-weakening relationships. In this regard they are good proxies for real earthquake ruptures, which might not always have linear slip-weakening curves. Although none of the following similarities was required in the optimization, both models have very similar distributions of slip, stress drop, and fracture energy.

The numerical resolution of model B is adequate for our purposes, but the numerical resolution of model A is not adequate for some purposes. Models A and B were calculated in numerical grids having rectangular subfaults of 0.8 km length and a depth-dependent width ranging from 0.3 km near the surface through 0.8 km between 4 and 10 km depth and increasing to 1.05 km at 12 km depth, with a time step of 0.069 sec. With this time sampling the breakdown duration for model B spanned seven or more time steps, as in Figure 1b for subfault 815. This subfault has one of the highest peak slip velocities in model B and is one of the most poorly resolved. Owing to model A's shorter D_c, the model A subfaults having highest peak slip velocity often have only one time sample during the breakdown process, which is inadequate resolution for an accurate calculation of D_c' from the unfiltered model A slip-velocity time series. Consequently, we cannot use the unfiltered model A slip-velocity time series to test the accuracy of D_c'. We can calculate D_c' for model B slip-velocity time series, but with a level of granularity less than or equal to that shown for subfault 815 in Figure 1 (which we believe to be acceptable, as we will show later). However, filtered rupture models A and B are valid numerical rupture models for their filtered seismograms. These models are better resolved and more finely sampled than most or all kinematic slip models derived from data, and we can test the effect of filtering on these numerical rupture models. It should be remembered that there is no real earthquake being simulated by models A and B. If there were, the D_c of unfiltered models A and B would probably overestimate the "true" D_c of the real earthquake owing to finite grid sizes and time steps.

Model A and B seismograms are very similar (Guatteri and Spudich, 2000, their figure 6). Figure 2 shows the amplitude and phase agreement of the model A and B seismograms in the 0- to 1-Hz band. We believe that this degree of agreement far exceeds the usual level of agreement between data and synthetics in inversions of strong-motion data. The agreement of amplitude spectra is almost perfect over the entire 0- to 1.0-Hz band. Also, the phase agreement is very good up to about 0.8 Hz, being less than an eighth of a cycle over most of that band. (A uniform time shift of 0.02 sec was applied to all model A seismograms before the phase difference was calculated.) Because of the excellent agreement shown in Figure 2, the filtered model A seismograms would be regarded as a good "fit" to the filtered B seismograms, and vice versa. Thus, both filtered slip models A and B would be readily accepted as slip models for either set of filtered seismograms.

Except when noted, we usually use a first-order low-pass Butterworth filter with a 1-Hz corner frequency, applied forward and backward (two-pass) to the slip-velocity time series, although in some calculations other corner frequencies are used. This specific filter was chosen to have a transfer function that is nonnegative to preserve the positivity of the filtered slip-velocity functions, and it was chosen to pass a frequency band in which the amplitude spectral ratios of the A and B seismograms is essentially unity. Weighted average breakdown time (weighted by each subfault's peak slip velocity) is 0.4 sec in model A and 1.9 sec in model B. Consequently, after low-pass filtering at 1.0 Hz, filtered model A becomes temporally unresolved whereas filtered model B remains temporally resolved.

Models A and B are useful models for testing the effect of bandwidth limitations on estimates of D_c because, despite having very similar seismograms, D_c for model B is about twice that for model A. Figures 3 and 4 show that D_c is roughly 0.35 m and 0.8 m in models A and B, respectively, for subfaults that slipped far enough so that their strength reached a plateau of dynamic friction (i.e., subfaults in which the maximum slip exceeds D_c). In panel *a* of both figures we show the results for all subfaults, whereas in panels *b* and *c* we show only the subfaults having peak slip speeds V greater than or equal to 60% or 80% of V_{max}, the peak slip speed of any subfault on the fault. We show these three sets of subfaults in these and subsequent figures to accentuate the behaviors of the subfaults having the highest slip velocities, which are the subfaults most likely to be considered significant in an inverted slip model. All the subfaults having $V \geq 0.6V_{max}$ have total slip exceeding 1.2 m, lie between depths of 9.6 and 12.1 km and between 17.5 and 21.6 km along strike, that is, in the rightmost slip maximum of figure 4 of Guatteri and Spudich (2000). These subfaults are far from

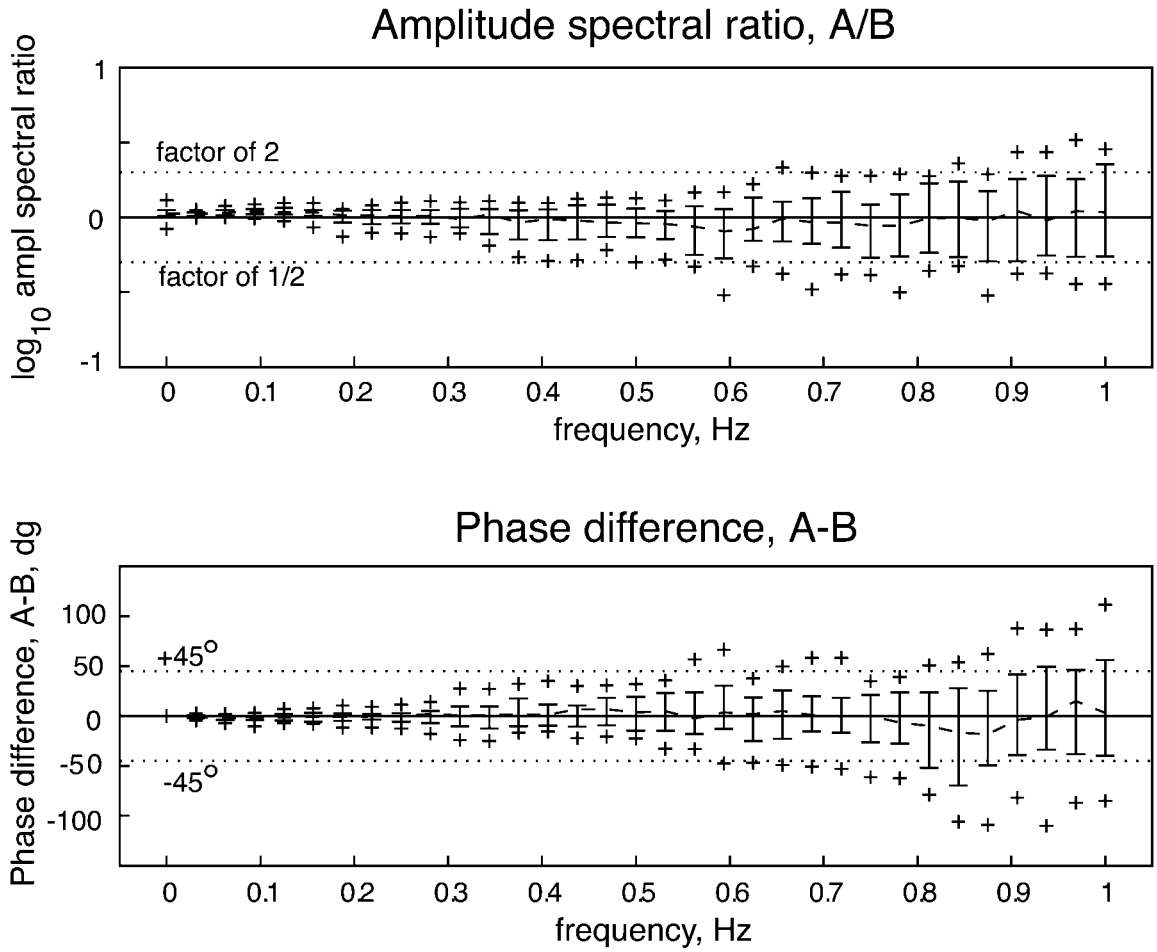

Figure 2. Comparison of model A and B seismograms in the frequency band 0–1 Hz. Dashed lines show medians, and error bars show upper and lower quartiles. Twenty percent of all values lie outside the + symbols. The upper panel shows the common logarithm of the A/B amplitude spectral ratios of all three components of motion at all 14 hypothetical seismograph locations. Dotted lines indicate a factor of 2. The lower panel shows the phase difference between A and B seismograms for all components at all locations. Dotted lines indicate 45° phase shifts.

the edges of the slip zone and far from regions of negative stress drop (black in Guatteri and Spudich [2000], figures 4c,d), and thus conform to the requirements for proper D_c' analysis.

Effect of Filtering on Slip-Weakening Curves

Low-pass filtering the slip-velocity and stress-change time functions can bias the inferred D_c toward the total slip, when using the method of Ide and Takeo (1997). Figure 5 shows the slip-weakening friction law inferred for subfault 815 after low-pass filtering slip velocity and stress change by two-pass first-order Butterworth filters having a variety of corner periods, $Tc = 0$ (no filter), 1, 2, and 3 sec. Low-pass filtering causes the sharp corner of the slip-weakening curve to disappear, and apparent slip-weakening distance rises toward the total slip amount. Physically, low-pass filtering the seismograms removes radiated energy from the seismograms, and the effect on the slip-weakening curves is to reduce the portion of the diagram that corresponds to radiated energy, namely, the region between the slip-weakening curve and the dashed line in Figure 5. Low-pass filtering might also bias the estimated fracture energy high and bias the radiated energy low by increasing the area under the slip-weakening curve, assuming that the stress level chosen as the boundary between fracture energy and heat is set at the final traction level. Radiated energy decreases as more energy is removed by filtering.

Effect of Filtering on D_c' Estimate

We use models A and B to answer the question of whether the D_c' parameter helps us to constrain D_c for real earthquakes for which we have a slip model derived from inversion of the observed ground motions. Because strong-motion data are usually low-pass filtered (often restricted to

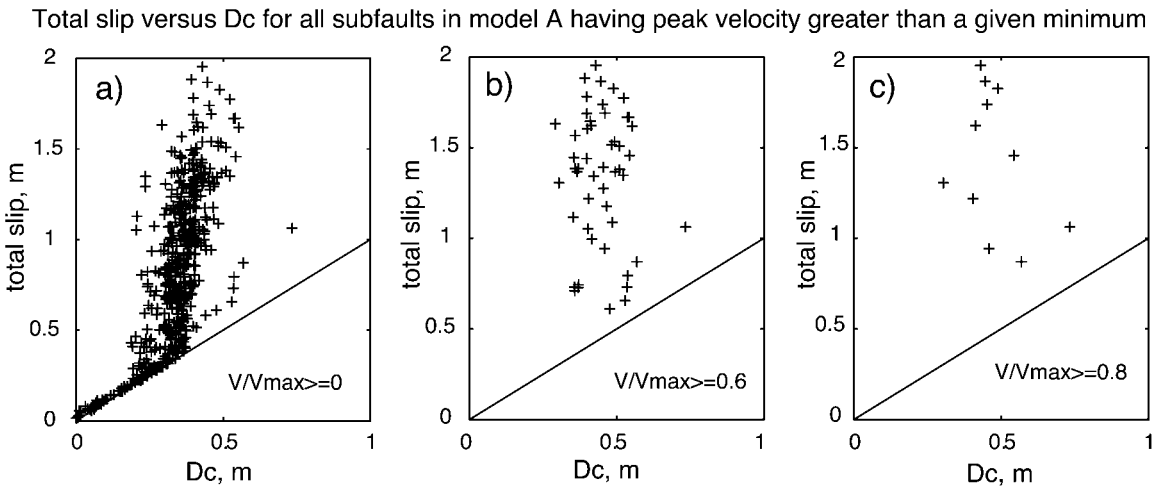

Figure 3. Total slip versus D_c for subfaults in model A having peak velocity V exceeding three different fractions of V_{max}, the maximum peak velocity anywhere on the fault. + signs are results for each subfault. The line indicates a 1:1 ratio. (a) All subfaults. Subfaults with total slip less than about 0.25 m did not weaken to a constant dynamic friction value. (b) Subfaults having peak velocity ≥60% of V_{max}. (c) Subfaults having peak velocity ≥80% of V_{max}. Note in b and c that D_c is independent of total slip.

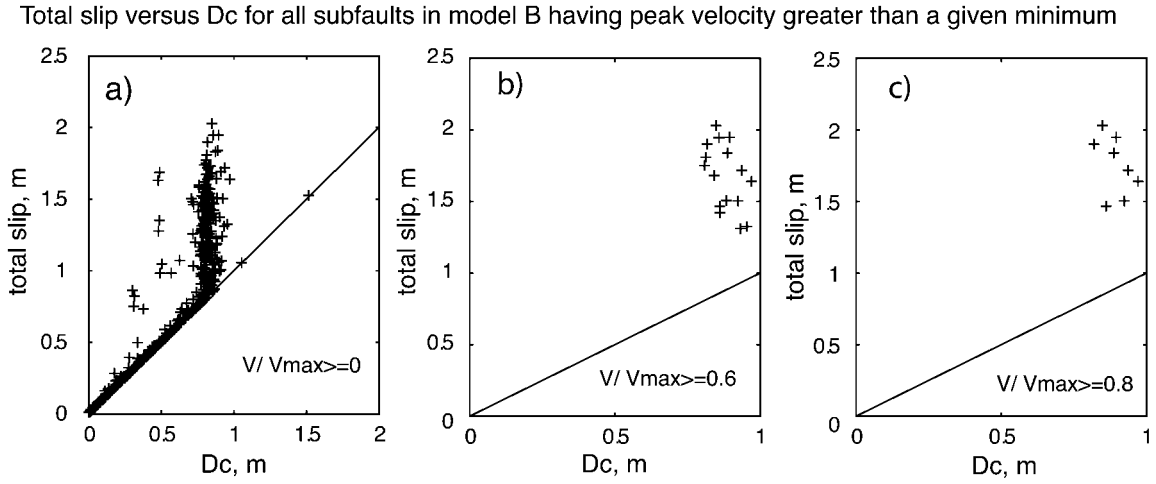

Figure 4. Total slip versus D_c for subfaults in model B having peak velocity V exceeding three different fractions of V_{max}, the maximum peak velocity anywhere on the fault. + signs are results for each subfault. The line indicates a 1:1 ratio. (a) All subfaults. Subfaults with total slip less than about 0.8 m did not weaken to a constant dynamic friction value. (b) Subfaults having peak velocity ≥60% of V_{max}, (c) Subfaults having peak velocity ≥80% of V_{max}. Note in b and c that D_c is independent of total slip.

the 0- to 0.5-Hz band), we low-pass filter the slip-velocity functions of models A and B, and we use these filtered slip models $f(t)*v(x,t)$ as surrogates for the slip models that would be obtained by inversion of filtered model A and B seismograms $f(t)*u(y,t)$. In fact, our low-pass-filtered slip models A and B still have perfect spatial resolution, and thus they are far more accurate than any inverted slip models. If D_c' shows biases in our low-pass filtered models A and B, then such biases might be even stronger in D_c' derived from inverted slip models.

The process of low-pass filtering strong-motion data (and the inferred slip models) can remove information about D_c, and the D_c' estimate does not recover the lost information. For temporally resolved model B the 1-Hz low-pass filter does not bias the D_c' estimate, as can be seen in Figure 6 by comparing the upper and lower rows. However, the effect

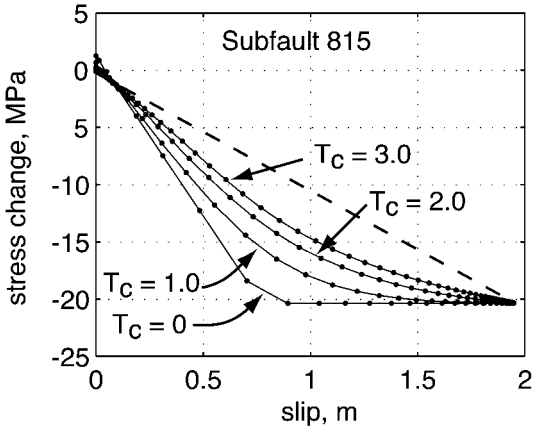

Figure 5. Effect of low-pass filtering on the apparent slip-weakening friction curve. T_c is the corner period of the filter. $T_c = 0$ sec is no filtering and is identical with Figure 1. Note that as progressively less low-frequency energy is passed by the filter, the apparent slip-weakening distance increases, approaching the total slip. Radiated energy is the area of the region between the diagonal line and the slip-weakening curve. Apparent fracture energy increases and radiated energy decreases as filter corner frequency decreases.

of filtering the slip models is to cause the D_c' estimates for models A and B to become equal, as can be seen in Figure 7 for all subfaults having peak velocity greater or equal to 60% of the maximum slip velocity anywhere on the fault. The + symbols in Figure 7 show that D_c for model B is about twice D_c for model A. However, the circles and × symbols show that as progressively heavier filtering is applied to models A and B, the D_c' estimates become very similar. This shows that D_c' derived from inverted slip models might be only an upper bound on D_c. We make two parenthetical comments. First, the upper right panel of Figure 6 shows the effect of granularity in the time step on resolution of D_c'. In some subfaults $D_c = D_c'$ exactly, and in other subfaults D_c differs from D_c' by one time step, as for subfault 815 in Figure 1. Second, although we have previously noted that the breakdown process for high-slip subfaults of model A is poorly resolved, we believe that the filter dependence of D_c' for model A shown in Figure 7 is not a consequence of the poor resolution, because model A is a valid numerical model for its ground motions, because a theoretical cause of the filter dependence will be given below, and because a similar filter dependence can be shown

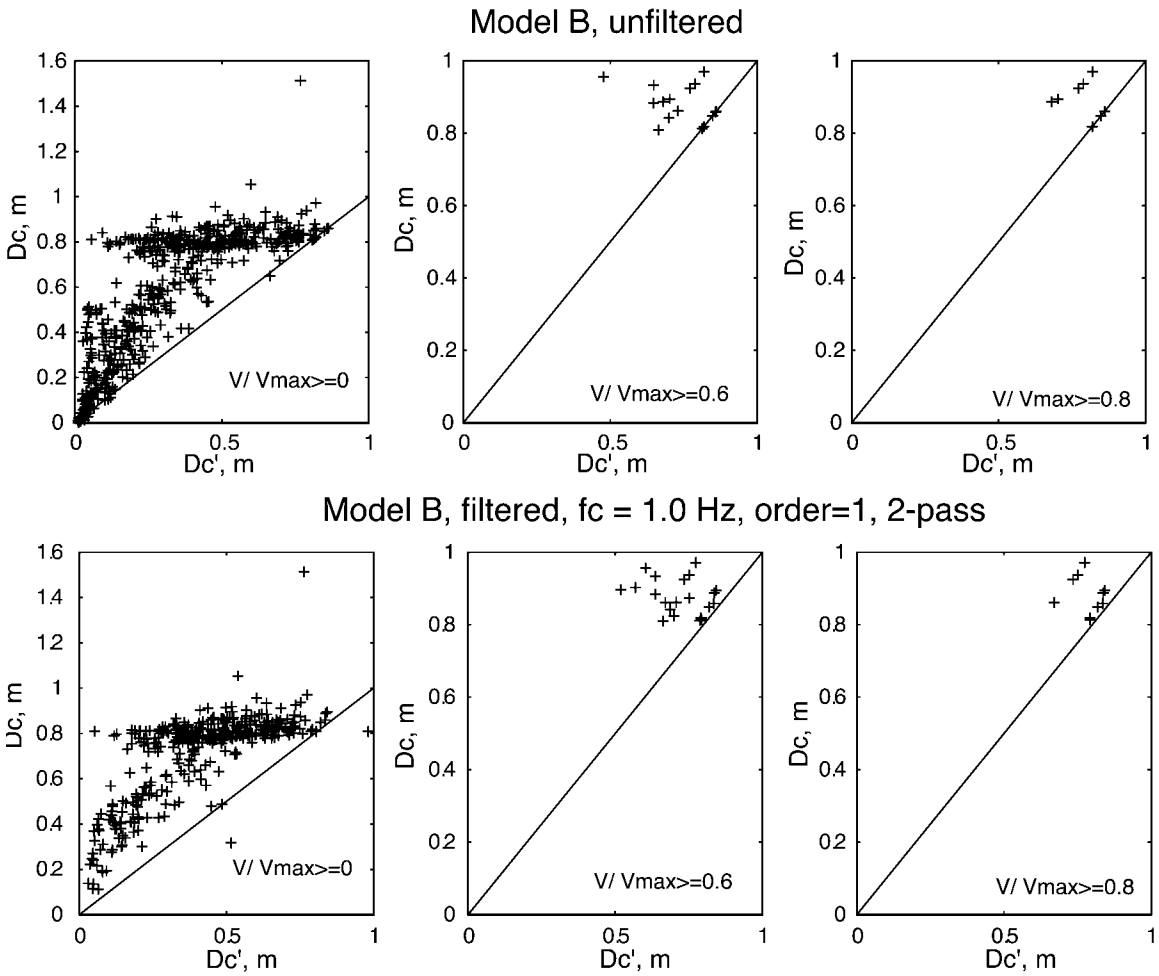

Figure 6. D_c versus D_c' for unfiltered slip model B (upper row) and low-pass-filtered slip model B (lower row). Filter is an acausal Butterworth having a 1-Hz corner frequency. Columns from left to right show all subfaults, subfaults having peak slip velocity ≥60% of the maximum and subfaults having peak slip velocity ≥80% of the maximum.

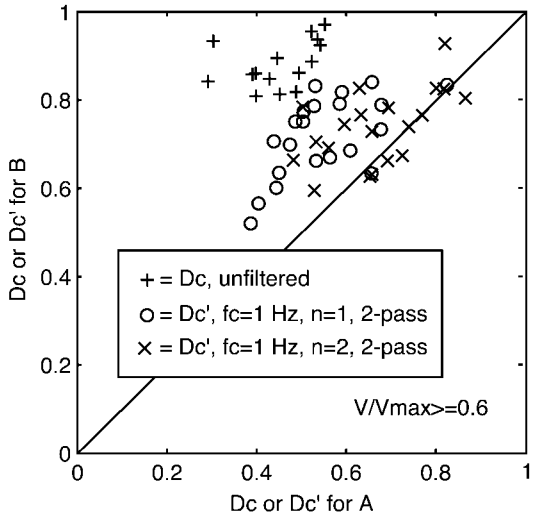

Figure 7. Comparison of D_c or D_c' in slip models A and B for subfaults having peak slip velocity ≥60% of V_{max}. + symbols show D_c for unfiltered slip models. Circles and × symbols show D_c' for slip models low-pass filtered at 1.0 Hz with two-pass, first-order or second-order, respectively, Butterworth filters. Note that progressively heavier low-pass filtering causes D_c' for models A and B to become equal.

to occur in more densely sampled results of Mikumo *et al.* (2003), as will be explained below.

Low-pass filtering can introduce an artificial correlation between D_c' and the total slip. Figure 8 shows the correlation of D_c' with total slip on each subfault in model B. For large slip-velocity subfaults D_c' is largely uncorrelated with total slip in the unfiltered model (upper row), but the filtering introduces a correlation between the two (lower row).

The artificial correlation between D_c' and the total slip is a consequence of the central limit theorem, which says that any positive function, when convolved by a large number of other positive functions, tends to a Gaussian. Thus, a slip-velocity function filtered sufficiently often becomes a Gaussian, in which half the slip occurs before the peak slip velocity, that is, $D_c' = D_{max}/2$, where D_{max} is the total slip of that subfault. Physically, causal and acausal filters tend either to shift the peak slip velocity later in time or move postpeak energy to a time before the peak. Both phenomena introduce the correlation. In other words, the D_c' estimate can be affected by slip that occurs after weakening is completed. We can demonstrate this phenomenon in a test using subfault 815. We first passed a piecewise cubic function through subfault 815's slip velocity time series, and then we interpolated with a sample period one-fourth of the original period. This interpolation was done to increase the resolution of any D_c' measurement. We then performed a second stage of interpolation designed to produce a set of slip-velocity functions each having the same D_c but having different D_{max}. This was accomplished by stretching, by various factors, the part of the slip-velocity function following the time sample having maximum slip velocity. In this second-stage interpolation (Figure 9) we interpolated the postpeak part of the slip-velocity time series by a different factor (larger, e.g., 2, 3, 4, and smaller, e.g., 1/2, 1/4), but we maintained the same nominal time step before and after the peak, so that interpolating by a factor of 3 lengthened the duration of the postpeak time series by a factor of 3. The effect of this was to produce several different slip-velocity time series, all having the same D_c', but having different total durations and different total slips. We applied a variety of low-pass filters to the time series, calculated D_c', and compared it with maximum slip (Fig. 10). That figure shows that D_c' is uncorrelated with total slip when there is no filtering, but D_c' becomes correlated with total slip when the slip-velocity time series is low-pass filtered. This is true for acausal and causal filters. This demonstration shows that the D_c' estimate can be affected by postbreakdown processes if the time series are filtered.

We have not attempted to correct our estimated D_c' for differences between breakdown time T_b and the time of peak velocity T, as advocated by Mikumo *et al.* (2003), for two reasons. First, their procedure is probably not applicable to our situation because, unlike their case with real earthquake data where true breakdown time T_b is unknown, we have the exact numerical rupture model and we know T_b exactly, so correction of unfiltered D_c' for the difference between T and T_b would yield D_c exactly. Second, their correction is independent of the passband of the filter used on the data, so any passband dependence of D_c' would remain in the corrected D_c'.

Discussion

Low-pass filtering a slip model can bias D_c inferred from stress-slip curves toward total slip, owing to the removal of radiated energy from the seismograms. This filtering might bias estimates of fracture energy upward and radiated energy downward, and it can introduce an artificial correlation of D_c' with total slip. Owing to the central limit theorem, a sufficiently heavily filtered slip-velocity function will tend toward a Gaussian, for which D_c' is half the total slip. In this regard it is interesting to consider the result of Zhang *et al.* (2003), who found for the 1999 Chi-Chi, Taiwan, earthquake that D_c, inferred from D_c' and from other methods, is correlated with total slip, with a constant of proportionality of 0.63. For the 2000 Tottori, Japan, earthquake we estimate that D_c' is about 0.45 of the maximum slip, based on the slope of a median straight line passed through the data in Figure 15 of Mikumo *et al.* (2003).

Our observed dependence of D_c' on filter corner in Figure 7 does not conflict with the independence observed by Mikumo *et al.* (2003, their figure 12). They performed their test using a causal second-order Butterworth filter (K. B. Olsen, personal comm.), whereas they filtered their data with a causal fourth-order Butterworth. The same test performed with a fourth-order Butterworth shows that D_c' increases to about 23 cm with a 0.5-Hz corner and to 35 cm with a 0.25-Hz corner. We performed this test by digitizing the 3-Hz

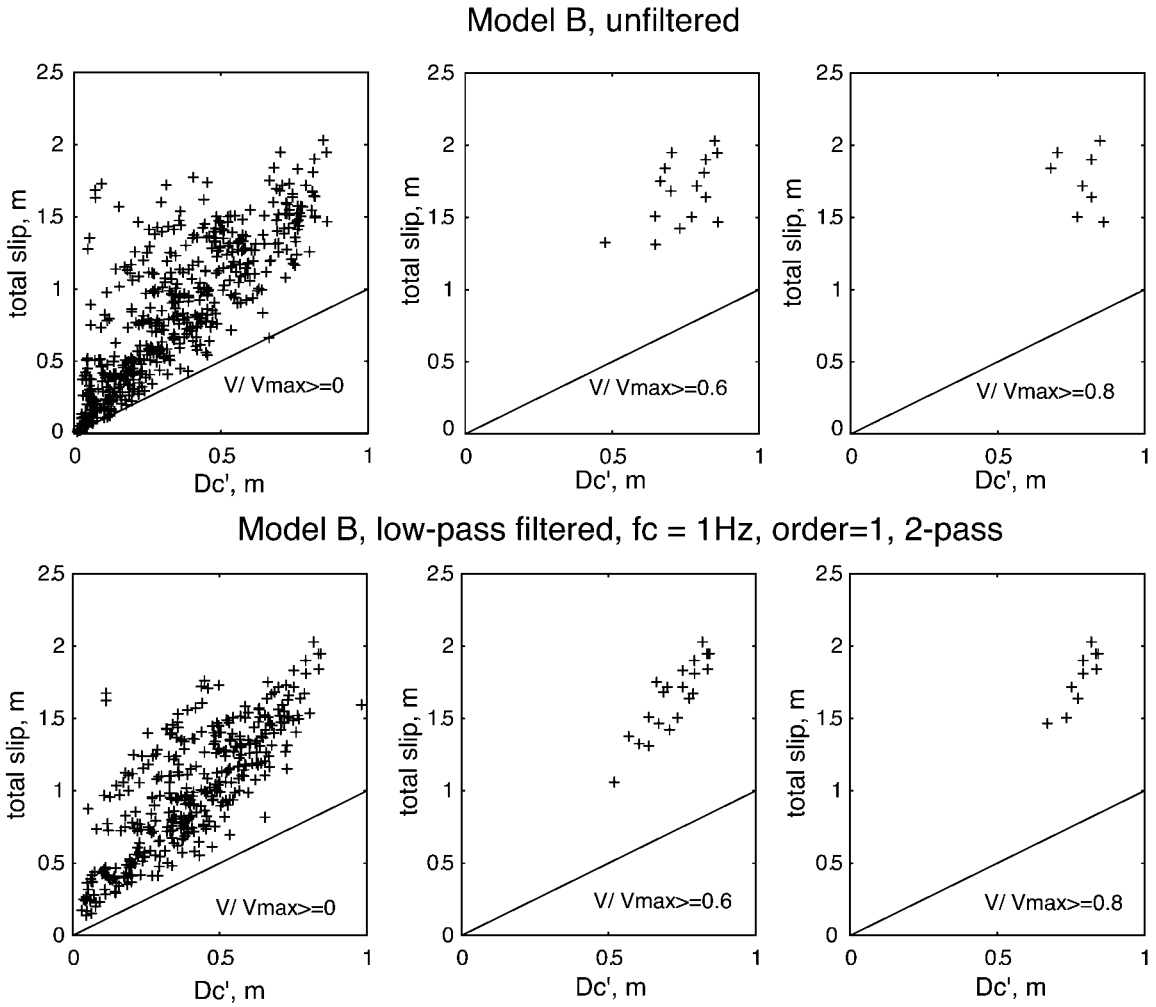

Figure 8. Correlation of D_c' with total slip for model B. The upper row shows an unfiltered slip model. The lower row shows a slip model low-pass filtered at 1.0 Hz. Columns, left to right, show subfaults having peak slip velocity ≥0%, 60%, and 80%, respectively, of V_{max}. Note that for high slip-velocity subfaults (right columns), low-pass filtering introduces a correlation between D_c' and maximum slip, even though the D_c' estimate is fairly good for low-pass-filtered model B.

filtered curve from their figure 12, deconvolving the 3-Hz second-order Butterworth and reconvolving with causal fourth-order Butterworth filters having a variety of corners.

To make progress, strong-motion modelers should routinely calculate and report the mistfit of their seismograms as a function of frequency, as has been done by Cotton and Campillo (1995) or as we have done in Figure 2. Quantitative calculation of misfits will make it clear that the frequency band in which the data are successfully modeled can be different from the passband of the filters used. Clearly the choice of a filter can bias inverted slip models, and the filter characteristics should be reported in detail. In addition, perhaps resolution of slip-weakening distance can be improved in ground-motion inversions by addition of a new constraint fixing the total radiated energy of a slip model to be a desired value determined from unfiltered local, regional, and global data.

Acknowledgments

We thank Takeshi Mikumo, Eiichi Fukuyama, and D. Joe Andrews for helpful comments and reviews.

References

Andrews, D. J. (1985). Dynamic plane-strain shear rupture with a slip-weakening friction law calculated by a boundary integral method, *Bull. Seism. Soc. Am.* **75,** 1–21.

Cotton, F., and M. Campillo (1995). Frequency domain inversion of strong motions: application to the 1992 Landers earthquake, *J. Geophys. Res.* **100,** 3961–3975.

Das, S., and B. V. Kostrov (1987). On the numerical boundary integral equation method for three-dimensional deynamic shear crack problems, *J. Appl. Mech.* **109,** 99–104.

Day, S., G. Yu, and D. Wald (1998). Dynamic stress change during rupture, *Bull. Seism. Soc. Am.* **88,** 512–522.

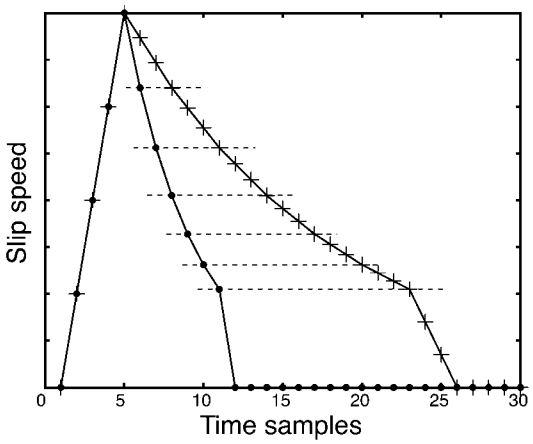

Figure 9. Schematic illustration of the way the postpeak part of the slip-velocity time function is stretched. Black dots show sampled slip velocity. In this example, three new samples are inserted by cubic interpolation between original samples (dots) following the peak. The postpeak, postinterpolation sample period is assumed to equal the prepeak sample period, effectively stretching the postpeak time series by a factor of 3 (crosses).

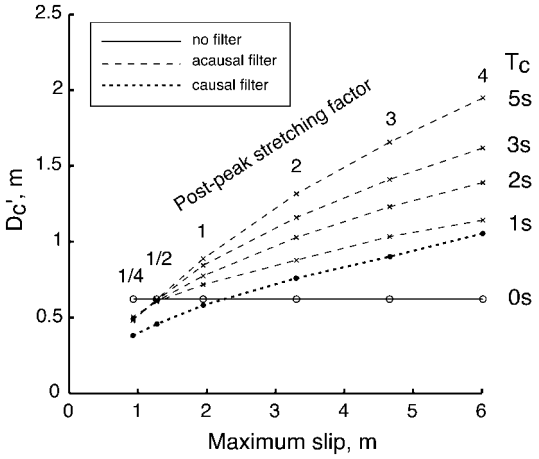

Figure 10. Comparison of model B D_c' and maximum slip for various stretched, filtered versions of the subfault 815 slip-velocity time series. Columns of points labeled "1/4, 1/2, . . ., 4" are the results of stretching the postpeak slip-velocity time series by the factors indicated. Each curve correponds to a different corner period of the filter. All filters are acausal (two-pass) first-order Butterworths, except the dotted line, which is causal (one-pass) first-order. When there is no filtering, D_c' is independent of maximum slip, but the D_c' values become correlated when the time series are filtered.

Fukuyama, E. , and T. Mikumo (1993). Dynamic rupture analysis: inversion for the source process of the 1990 Izu Oshima, Japan earthquake (M6.5), *J. Geophys. Res.* **88,** 2191–2198.

Fukuyama, E., T. Mikumo, and K. B. Olsen (2003). Estimation of the critical slip-weakening distance: Theoretical background, *Bull. Seism. Soc. Am.* **93,** 1835–1840.

Guatteri, M., and P. Spudich (2000). What can strong motion data tell us about slip-weakening fault-friction laws?, *Bull. Seism. Soc. Am.* **90,** 98–116.

Ide, S., and M. Takeo (1997). Determination of constitutive relations of fault slip based on seismic wave analysis, *J. Geophys. Res.* **102,** 27,379–27,391.

Mikumo, T., K. B. Olsen, E. Fukuyama, and Y. Yagi (2003). Stress-breakdown time and slip-weakening distance inferred from slip-velocity functions on earthquake faults, *Bull. Seism. Soc. Am.* **93,** 264–282.

Zhang, W., T. Iwata, K. Irikura, H. Sekiguchi, and M. Bouchon (2003). Heterogeneous distribution of the dynamic source parameters of the 1999 Chi-Chi, Taiwan, earthquake, *J. Geophys. Res.* **108,** 2232, doi 10.1029/2002JB001889.

U.S. Geological Survey
345 Middlefield Road
Menlo Park, California 94205
spudich@usgs.gov
(P.S.)

Swiss Re
175 King St.
Armonk, New York 10504
Mariagiovanna_Guatteri@swissre.com
(M.G.)

Manuscript received 30 May 2003.